Solubility of 1:1 Alkali Nitrates and Chlorides in Near-Critical and Supercritical Water

ARTICLE *in* JOURNAL OF CHEMICAL & ENGINEERING DATA · JULY 2009

Impact Factor: 2.04 · DOI: 10.1021/je900175b

Chapter 4

The solubility of 1:1 alkali nitrates and chlorides in near-critical and supercritical water

This chapter has been published as:
Leusbrock, I., Metz, S. J., Rexwinkel, G., and Versteeg, G. F. (2009); *Solubility of 1:1 Alkali Nitrates and Chlorides in Near-Critical and Supercritical Water*; Journal of Chemical & Engineering Data 54(12), 3215-3223.

Abstract

To increase the available data on systems containing supercritical water and inorganic compounds, an experimental setup was designed to investigate the solubilities of inorganic compounds in supercritical water. In this work, three alkali chloride salts (LiCl, NaCl, KCl) and three alkali nitrate salts ($\mathrm{LiNO_3}$, $\mathrm{NaNO_3}$, $\mathrm{KNO_3}$) were investigated in the range from 653 to 693 K and from 18 to 23.5 MPa. The experimental results were correlated with a model based on the phase equilibrium between the inorganic compound and supercritical water. When available, the experimental data was extended with data available in the open literature. The experimental results and parameters obtained by this model were compared with each others and evaluated under consideration of the physical aspects of the inorganic compounds. In addition to the main purpose of the experiments, side reactions like decomposition of nitrate and changes in pH were observed and discussed in this work.

The presented data is the first coherent study of the solubility of six common inorganic compounds in one setup and with one method.

Keywords: Alkali chlorides, Alkali nitrates, Phase equilibrium, Salt, Solubility, Supercritical water

4.1 Introduction

Supercritical fluids receive more and more attention in science and industry due to the versatile application possibilities. This versatility is based on the adjustable properties of supercritical fluids (1). The applications for supercritical fluids range from extraction, particle formation, reactions, cleaning to dyeing (2–10).

Supercritical water as a medium for industrial applications has received little attention in literature and research so far since the critical properties (T_c = $647 K$, p_c = $22.1 MPa$) result in harsher conditions for materials and equipment. This results in limited knowledge of the properties of supercritical water systems and mixtures of supercritical water and organic / inorganic compounds compared to other fluids (e.g. carbon dioxide). Nevertheless, several new approaches and research projects recently started to use supercritical water as a solvent of choice due to the beneficial aspects of supercritical water (e.g. inexpensive and green solvent, high thermal capacity, diffusion adaptability, changing solvation behavior). These projects include reactions in supercritical water (11–14), gasification of biomass in supercritical water (15–17), oxidation of waste material in supercritical water (18–21) and the removal of inorganic compounds in supercritical water. To improve and to optimize these new approaches, additional data and understanding of the system is necessary (22).

One important aspect for all these approaches is the presence of inorganic compounds (e.g. salts) in the supercritical system. The solubility of these compounds is tremendously diminished in comparison to the solubility at ambient conditions (23; 24). The reason for this is the different structure of supercritical water and the reduced dielectric constant. This leads to weaker hydrogen bonding and to less hydration of the inorganic molecules by the surrounding water molecules (25; 26). Due to this behavior, water changes from an excellent solvent for inorganic compounds at ambient conditions to a poor one at supercritical conditions. As a result of the diminished solubility, the inorganic compounds start to precipitate and to form a solid phase within the supercritical water system.

The presence of a solid phase may lead to problems within the system. Blocking of parts of the equipment may occur as well as the deposition of solid particles on the walls of the equipment (27–29). This can result in an increased pressure drop along the system and end up in a total failure. Additionally, erosion and corrosion are negative side effects of the presence of a solid phase, especially if the material used is not designed or capable to deal with corrosion (30–33). On the other hand, the diminished solubility

of inorganic compounds can be used to remove these compounds from the water phase or the different solubilities of different salts can be applied to separate the salt fractions from each other.

In order to obtain further insight in the properties of salt + supercritical water systems, three alkali nitrate salts ($LiNO_3$, $NaNO_3$, KNO_3) and three alkali chloride salts ($LiCl$, $NaCl$, KCl) were investigated systematically regarding their solubility and behavior. The investigated temperature and pressure range was 653 to 693 K and from 18 to 23.5 MPa. These two sets differ in the type of the cation. The effect of the type of cation and anion were studied by comparison of the experimental results. The results of the experiments were evaluated using a model based on the description of the phase equilibrium between the solid phase and the supercritical fluid phase (34; 35). The parameters obtained with this model are compared and a correlation between these parameters and the properties of the solids is proposed. Furthermore, several aspects like possible side reactions during the experiments as well as changes in pH are mentioned and discussed.

4.2 Theoretical background

4.2.1 Solubility in supercritical water

For the interpretation of the solubility experiments, a model derived from the description of the equilibrium between the two present phases, solid and supercritical fluid, is applied (24; 35–37). A phase diagram with the solubility of $NaCl$ as a function of the density of water is shown in 4.1. This equilibrium can be interpreted as follows:

$$a \cdot Me^c \ * \ m \cdot H_2O(f) + b \cdot X^d \ * \ p \cdot H_2O(f) \rightleftharpoons Me_aX_b \ * \ n \cdot H_2O(f) \quad (4.1)$$

$$Me_aX_b \ * \ n \cdot H_2O(f) \rightleftharpoons Me_aX_b(s) + n \cdot H_2O(f) \quad (4.2)$$

Me represents the salt cation while X represents the salt anion; a and b are the number of ions in the salt molecule, c and d its valency. n, m and p are the number of water molecules needed for solvation for the salt and the ions while s and f refer to the phases solid and fluid. Regarding the equilibrium, it is assumed that the formation of a solid only takes place via the associated complex and not via the dissociated salt ions.

A formulation of the phase equilibrium constant K_s leads to the following expression:

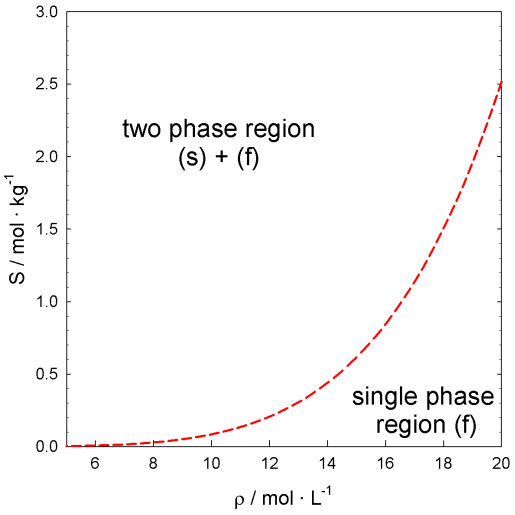

Figure 4.1 ‖ Solubility curve of NaCl(24)

$$K_s = \frac{\alpha_{Me_aX_b * n \cdot H_2O(f)}}{\alpha_{Me_aX_b(s)} \cdot \alpha^n_{H_2O(f)}} \tag{4.3}$$

α refers to the activity of the species on a molality base.

Several assumptions can be made to simplify this expression. The activity coefficient of the solid salts is considered as unity. Interaction between the presented species is neglected. For the fluid water phase, an ideal behavior is assumed. These assumptions have been used successfully to describe the solubility of inorganic compounds in supercritical fluids (24; 34; 35).

For a more convenient interpretation of the parameters, a description on an amount of substance base is chosen. The density of water is described as amount of substance density, while the composition is given as molality. The density of pure water is calculated via the IAPWS95 equation of state (38).

A more detailed explanation on the assumptions can be found in a previous work of the authors (34).

$$K^*_s \approx \frac{m_{Me_aX_b * n \cdot H_2O(f)}}{1 \cdot \rho^n_{m,\, H_2O(f)}} \tag{4.4}$$

$$\Longrightarrow \quad m_{Me_aX_b * n \cdot H_2O(f)} = K^*_s \cdot \rho^n_{m,\, H_2O(f)} \tag{4.5}$$

The equilibrium constant for the simplified form of the equilibrium, K^*_s, can be also expressed under usage of a van't-Hoff like expression as:

$$K_s^* = \exp\left(-\frac{\Delta_{solv}\, G}{R \cdot T}\right) \tag{4.6}$$

$$= \exp\left(-\frac{\Delta_{solv}\, H}{R \cdot T} + \frac{\Delta_{solv}\, S}{R}\right) \tag{4.7}$$

$$\Longrightarrow \log\, m_{Me_aX_b * n \cdot H_2O} = \log K_s^* + n \cdot \log \rho_{m,\, H_2O} \tag{4.8}$$

$$= -\frac{\Delta_{solv}\, H}{R \cdot T} + \frac{\Delta_{solv}\, S}{R} + n \cdot \log\, \rho_{m,\, H_2O} \tag{4.9}$$

R is the universal gas constant, T the system temperature, m the molality. For the Gibbs energy of solvation, $\Delta_{solv}\, G$, the enthalpy of solvation, $\Delta_{solv}\, H$, and the entropy of solvation, $\Delta_{solv}\, S$, it is assumed that they are independent of the system parameters temperature, pressure and density. n is later on referred to as the coordination number. To indicate the assumption of an independence of the enthalpy of solvation and the entropy of solvation from the system properties, equation 4.9 is formulated as follows:

$$\log\, m_{Me_aX_b * n \cdot H_2O} = -\frac{A}{R \cdot T} + \frac{B}{R} + n \cdot \log\, \rho_{m,\, H_2O} \tag{4.10}$$

The validity and the applicability of this approach for the interpretation of the salt + supercritical water system has been shown elsewhere (34). In this previous work, Eq. 4.9 respectively 4.10 has been compared and evaluated to several further approaches from literature.

4.3 Experimental

4.3.1 Experimental setup

For the measurement of the solubilities, an experimental setup was designed (cf. Fig. 4.2). The operation range of the setup is up to 25 MPa as well as up to 723 K. To avoid corrosion and to guarantee to withstand the mechanical and thermal stress of the conditions, Hastelloy is used for all parts that are in contact with the heated medium. The pressure is provided by a HPLC pump (LabAlliance Series III) with a volume flow of 0.1 to 10 $mL \cdot min^{-1}$. The temperature is provided by a custom-made oven which is supported by an electrical pre-heater. Inside the oven, a U-tube is installed in which the precipitation takes place. The inner diameter of the tube is 4.6 mm, the outer diameter 6.35 mm and the length 265 mm. The temperature along this tube is measured at three different positions with standard PT100 thermocouples (relative uncertainty 0.25

%). The pressure inside the setup is measured with a pressure sensor (Keller PA23H, relative uncertainty 0.2 %) Behind the tube, a filter (Pore size 0.5 μm) is installed to prevent any particles from being entrained to later sections.

The analysis of the samples is done via an inductive coupled plasma atom emission spectrometer (Perkin-Elmer Optima 5300DV, relative uncertainty < 2 % for all investigated species) for the cation composition and liquid chromatography (Metrohm 741 Compact IC, relative uncertainty < 5 % for all investigated species) for the anion composition. The pH values of the samples were measured with a standard pH electrode (WTW pH/Cond 340i/SET; uncertainty after calibration ± 0.01). The process data is logged continuously for later interpretation of the results.

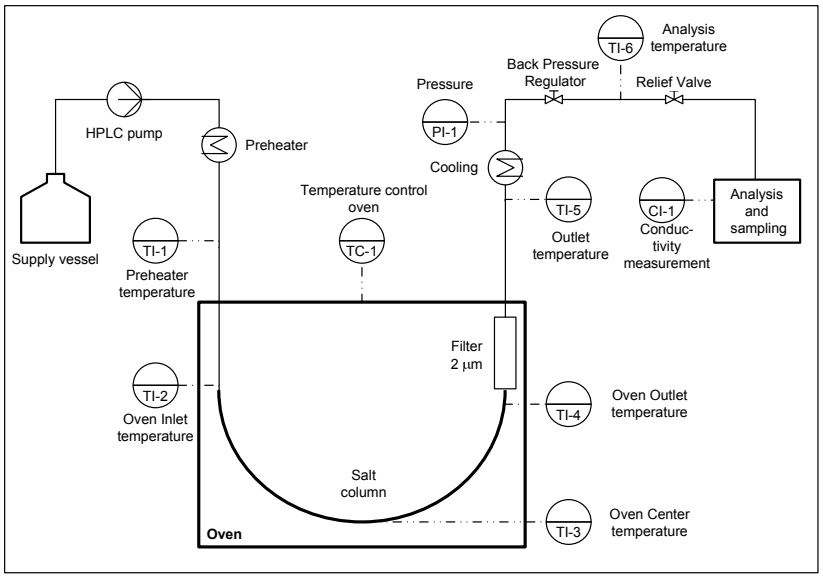

Figure 4.2 ‖ Flow scheme of the experimental setup

4.3.2 Experimental procedure

As a feed stream, deionized water plus a known amount of salt were used. The salt that were used were of high purity (> 99.5 %). The salt concentration in the feed was 0.05 $mol \cdot L^{-1}$. The volume flow was 1 $mL \cdot min^{-1}$ for the experiments with NaCl, for the other salts 0.5 $mL \cdot min^{-1}$. The resulting residence time was appr. 260 s respectively 520 s. The temperature and pressure in the column were adjusted to the desired conditions. The temperature was kept constant for the duration of the whole experiment while the pressure was reduced stepwise after taking samples at each measurement point.

Upon entering the column, the stream can be oversaturated due to the conditions in the column and the investigated salt. If a oversaturation occurs, precipitation of the salt will take place until the phase equilibrium between both phases is established in the column. The resulting stream leaves the system at the solubility resulting from the temperature and pressure in the column. The stream is cooled down and depressurized to ambient conditions.

Next to the other properties, the conductivity of the outlet stream is measured. If the conductivity and thereby the composition was constant for a longer period of time (t $\geq$ 10 min), an equilibrium state in the column was assumed. If the system reaches such a constant state, two samples were taken in an interval of 30 min. These samples are analyzed regarding their composition with the analytical methods mentioned above. For the calculation of the density, the outlet temperature (TI-4 in Fig. 4.2) and the pressure at the pressure sensor (PI-1 in Fig. 4.2) were used. Pressure drops between the U-tube and the pressure sensor were neglected due to the low volume flows. Plugging inside in the U-tube was avoided by the low feed concentration and the (in comparison the feed concentration) large volume of the U-tube.

A more extensive description of the setup and the procedure can be found elsewhere (34).

4.4 Results and discussion

In order to increase the available property data of inorganic compounds in supercritical water, two sets of salts were systematically investigated, alkali nitrate and chloride salts. Each set is distinguished by the type of cation: lithium, sodium and potassium. Each salt was investigated regarding its solubility with the same setup and method. For several of these salts, almost no literature data was available till this point.

4.4.1 Nitrate salts

Three alkali nitrate compounds were investigated: $\mathrm{LiNO_3}$, $\mathrm{NaNO_3}$ and $\mathrm{KNO_3}$. Several properties of these salts are listed in Table 4.1 (39; 40). The molecule radius is the sum of the crystal radius of the anion and the cation (40). The melting temperatures of all nitrates are below the investigated temperature range resulting in the nitrate salts being in a liquid state during the experiments.

In Figure 4.3, 4.4 and 4.5, the experimental data on the different nitrate salts is

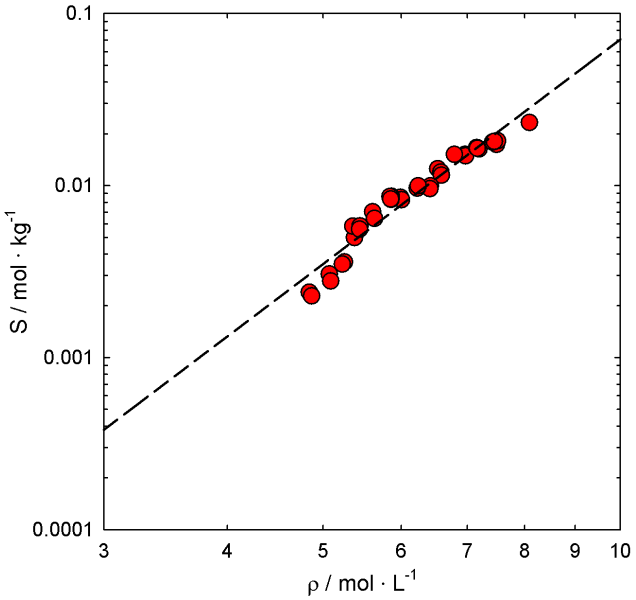

Figure 4.3 ‖ Solubility of $LiNO_3$ as function of density; ∘, this work; dashed line represents the description of the experimental data with Eq. 4.10; parameters are listed in Tbl. 4.2

Table 4.1 ‖ Properties of $LiNO_3$, $NaNO_3$, and KNO_3

Salt	T_{fus} / K (39)	M / $g \cdot mol^{-1}$ (39)	r / $10^{-12}m$ (40)
$LiNO_3$	537	68.95	352
$NaNO_3$	580	84.99	392
KNO_3	607	101.11	430

presented. The solubility of each compound is presented as a function of the density of pure water, thereby as a function of temperature and pressure. The experimental data covers a density range of 4 to 9 $mol \cdot L^{-1}$ (appr. 17 to 23.5 MPa, 650 to 700 K). Where available, solubility data from the literature was added to the experimental data (41). As can be seen from the figures, the measurements presented in this work agree well with the results in the literature. The experimental data including temperature and pressure as well as their standard deviations, the density, the composition and the pH for the measurements on the nitrate salts can be found in the supporting information.

The three parameters of Eq. 4.10, A, B and n, were fitted to the experimental data by application of the software MATLAB. For the fitting procedure, the cation composition was used as solubility in consistence with previous works (24; 34; 42). All experimental

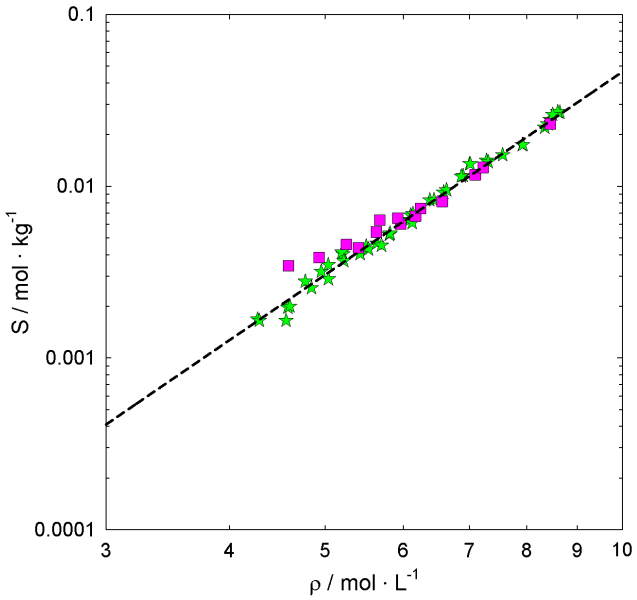

Figure 4.4 ‖ Solubility of $NaNO_3$ as function of density; ⋆, this work; □, Dell'Orco et al. (41); dashed line represents the description of the experimental data with Eq. 4.10; parameters are listed in Tbl. 4.2

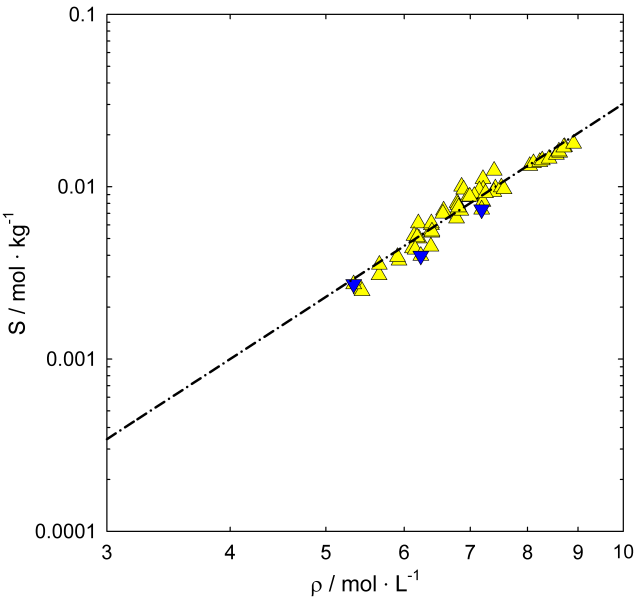

Figure 4.5 ‖ Solubility of KNO_3 as function of density; △, this work; ▽, Dell'Orco et al. (41); dashed line represents the description of the experimental data with Eq. 4.10; parameters are listed in Tbl. 4.2

data can be described with good agreement with the model presented (34). The obtained parameters for this model are listed in Table 4.2 and will be discussed in the following section.

Table 4.2 ‖ Parameters for the description of the solubilities of $\mathrm{LiNO_3}$, $\mathrm{NaNO_3}$, and $\mathrm{KNO_3}$ with Eq. 4.10

Salt	A / $J \cdot mol^{-1}$	B / $J \cdot mol^{-1} \cdot K^{-1}$	n / -
$\mathrm{LiNO_3}$	15594	-81.91	4.33
$\mathrm{NaNO_3}$	5149	-93.06	3.93
$\mathrm{KNO_3}$	-7793	-111.91	3.72

4.4.2 Chloride salts

Three alkali chloride compounds were investigated: LiCl, NaCl and KCl. Several properties of these salts are listed in Table 4.3 (39; 40).

In Figures 4.6, 4.7 and 4.8, the experimental data on the different nitrate salts is presented. The solubility of each compound is presented as a function of the density of pure water, thereby as a function of temperature and pressure. The experimental data covers a density range of 4 to 9 $mol \cdot L^{-1}$ (appr. 17 to 23.5 MPa, 650 to 700 K). Where available, solubility data from literature was added to experimental data from this work (24; 42; 43). As can be seen from the figures, the measurements presented in this work agree well with the results in literature. The experimental data for the measurements on the chloride salts can be found in the supporting information. The experimental data for NaCl can also be found in Table B.1 in Appendix B. For the measurements of NaCl, a scatter in the solubility results has to be mentioned.

All experimental data can be described with good agreement with the presented

Table 4.3 ‖ Properties of LiCl, NaCl and KCl

Salt	T_{fus} / K (39)	M / $g \cdot mol^{-1}$ (39)	r / $10^{-12}m$ (40)
LiCl	886	42.4	240
NaCl	1074	58.45	280
KCl	1049	74.55	318

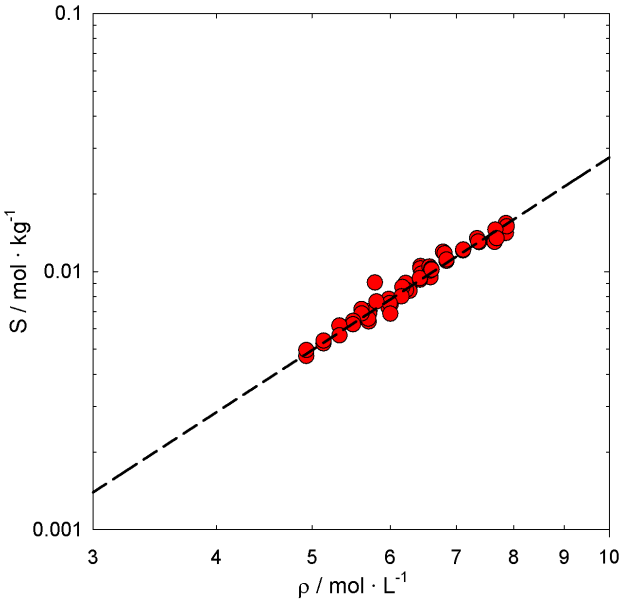

Figure 4.6 ‖ Solubility of LiCl as function of density; ∘, this work; dashed line represents the description of the experimental data with Eq. 4.10; parameters are listed in Tbl. 4.4

Table 4.4 ‖ Parameters for the description of the solubilities of LiCl, NaCl, and KCl with Eq. 4.10

Salt	A / $J \cdot mol^{-1}$	B / $J \cdot mol^{-1} \cdot K^{-1}$	n / -
LiCl	5199	-69.61	2.48
NaCl	18784	-86.74	4.88
KCl	13123	-95.66	4.65

model. The parameters obtained with this model are listed in Tbl. 4.4.

4.4.3 Side reactions in SCW

In all experiments with nitrate salts, a small amount of nitrite was found in the samples. Since the feed solutions were produced by using very pure nitrate salts, it can be assumed that a decomposition of nitrate to nitrite took place.

$$2\,\mathrm{XNO_3} \leftrightharpoons 2\,\mathrm{XNO_2} + \mathrm{O_2} \tag{4.11}$$

The molality of nitrite in the experiments with $\mathrm{LiNO_3}$, $\mathrm{NaNO_3}$, and $\mathrm{KNO_3}$ were determined as between 0.0005 and 0.0015 $mol \cdot kg^{-1}$. These results on the nitrite com-

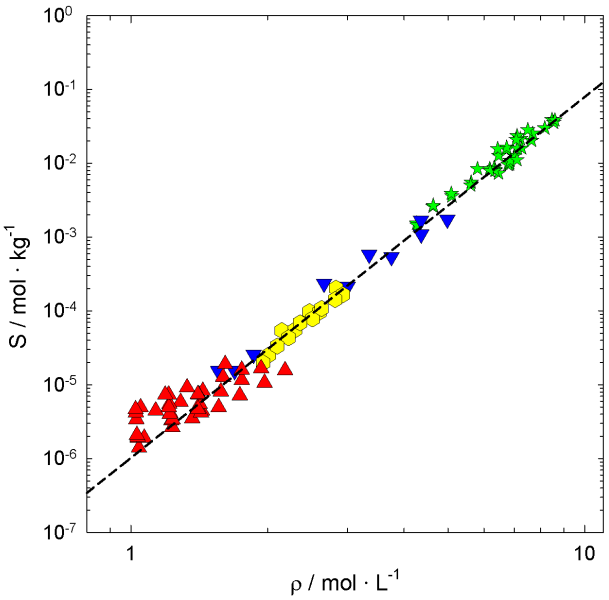

Figure 4.7 ‖ Solubility of NaCl as function of density; $\star$, this work; $\triangledown$, Armellini et al. (24); $\hexagon$, Higashi et al. (42); $\triangle$, Galobardes et al. (43); dashed line represents the description of the experimental data with Eq. 4.10; parameters are listed in Tbl. 4.4

position show a relatively experimental high uncertainty [1] due to the low concentrations. Yet the qualitative result of these observations, the decomposition from nitrate to nitrite, is without doubt. Although only a rather small temperature range from 650 to 700 K was investigated, a higher decomposition of nitrate to nitrite can be expected at higher temperatures. Especially, the presence of oxygen might lead to problems in applications since corrosion is enhanced by the presence of oxygen.

In all experiments, a decrease in pH from 4 to 6 was measured. Due to the only slightly acidic feed solutions, pH 6.7 to 6.9, for all salts, a hydrolysis of the salt is considered as the reason for the drop in pH (24; 41; 43). The equilibrium of the hydrolysis is favorable to higher temperatures / lower densities (cf. Fig. 4.9). The possible reaction mechanism is depicted below:

$$\mathrm{XCl} + \mathrm{H_2O} \rightleftharpoons \mathrm{XOH}(s)\downarrow + \mathrm{HCl} \tag{4.12}$$

$$\mathrm{XNO_3} + \mathrm{H_2O} \rightleftharpoons \mathrm{XOH}(s)\downarrow + \mathrm{HNO_3} \tag{4.13}$$

[1] Multiple analyses of the same sample showed deviations in the range of 10% in nitrite composition from each other. This was caused by operating at the lower end of the detection limit of the analytical method.

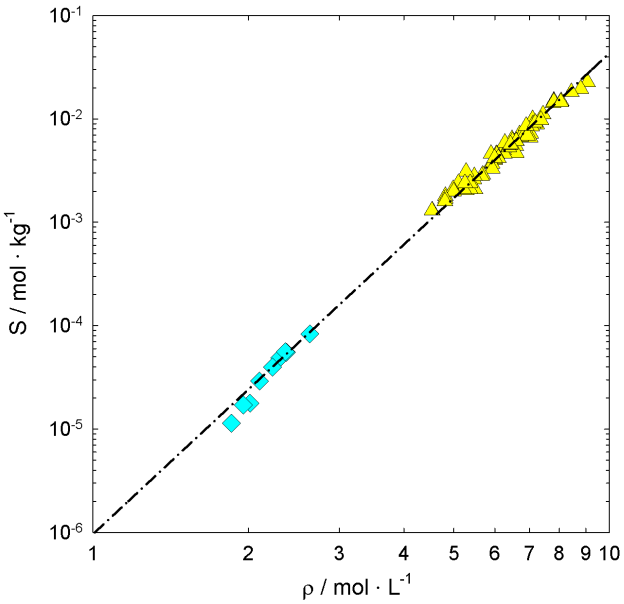

Figure 4.8 ‖ Solubility of KCl as function of density; △, this work; ⋄, Higashi et al. (42); dashed line represents the description of the experimental data with Eq. 4.10; parameters are listed in Tbl. 4.4

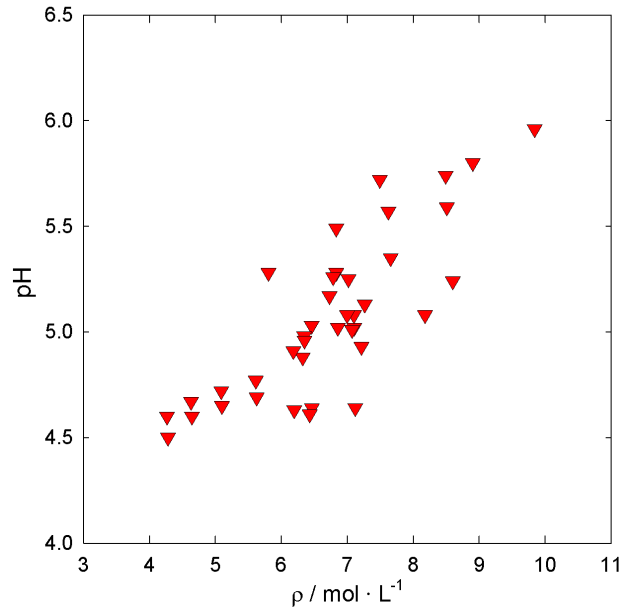

Figure 4.9 ‖ Measured pH of the experiments with NaCl as a function of the density

The hydroxide precipitates and remains in the column. From this reaction the outlet stream becomes acidic due to the presence of HCl / $\mathrm{HNO_3}$. This fact is supported by

the ratio of the cation and the anion concentrations in the samples. Here the ratio of anion to cation is usually slightly higher than 1 which indicates a surplus of anions due to the hydrolysis. Therefore, the cation composition of the outlet stream correspond to the solubility of the investigated salt if the hydrolysis is taken into account. Yet the pH change is small resulting in small differences between the anion and cation composition. This decrease in pH for all salt solutions has to be kept in mind for applications where corrosion must be prevented and the water stream is used afterwards for further purposes.

During the evaluation of the experimental data, it has been not accounted and corrected for the side reactions. It is assumed that at pH 4 a maximum deviation in the solubility results of 5 $\%$ due to the side reactions occurs.

4.4.4 Discussion

In Figure 4.10, the solubilities of the nitrate salts are compared. A trend in the solubilities can be clearly seen so that a tendency in the solubility of alkali nitrate salts can be determined ($\mathrm{LiNO_3} > \mathrm{NaNO_3} > \mathrm{KNO_3}$). This tendency has also been assumed by other groups, yet the available experimental data was scarce (41). To explain this tendency, the radii of the salt molecules can be taken into consideration. Due to the changed physical properties of water in its supercritical state and the therefore diminished dielectric constant, the solvation power of water is reduced and the hydrogen bonds are weakened (26). As one result, this leads to an association of the ions (25; 34; 44). As further effect, the hydration of the molecules decreases due to the weakened hydrogen bonds (25; 26). Additionally, the hydrogen bonding between the water molecules competes strongly with the actual solvation of the solutes and thereby decreases the solvation ability of supercritical water (45). As a result, the molecules cannot be kept in solution and start to form a solid phase.

Table 4.1 contains the radii of the associated nitrate salts with the cation being the only difference. As can be seen from this table and Table 4.10, a higher solubility corresponds with a smaller radius. Here, the difficulty in hydration of the salt molecule is considered as a possible reason for this relation. It is easier to maintain the hydration sphere around a smaller molecule and to keep it in solution. This results from the reduced distance between the water molecules to establish hydrogen bondings with other water molecules and the salt molecule and to maintain them.

The parameters of approach Eq. 4.10 - A, B and n - for the investigated nitrate salts are listed in Table 4.2. The coordination number n decreases from 4.33 for $\mathrm{LiNO_3}$

to 3.72 for KNO_3 in correspondence with decreasing solubility and increasing radius. The coordination number can be taken as an indication on how far it is still possible to solvate the salt molecule. If a salt molecule can bind more water molecules in its hydration sphere like $LiNO_3$, its solubility is higher than in comparison with KNO_3. For KNO_3, it is apparent that the larger radius and the changed properties lead to a lower concentration of water molecules around the salt molecule. Therefore, the solubility and the coordination number are lower.

In Figure 4.11, the solubility of the chloride salts are compared. The experimental data of $NaCl$ shows in comparison to the other salts scatter in the composition results. The experiments on $NaCl$ were the first to be performed with the setup, thereby adding ann additional uncertainty. Contrary to the nitrate salts, no clear trend can be seen. While $NaCl$ and KCl behave according to the corresponding nitrate salts, $LiCl$ shows a lower solubility for densities $\geq 6\,\mathrm{mol}\cdot\mathrm{L}^{-1}$ than one could assume based on the previous results.

A possible explanation for this anomalous behavior is assumed to result from the nature of lithium itself. With lithium being the lightest of the metals and having the smallest ionic radius, several abnormal phenomena in comparison to other alkali metals

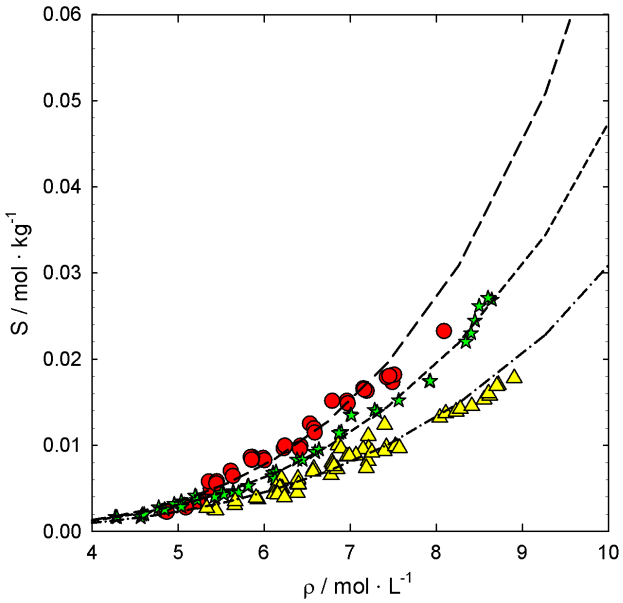

Figure 4.10 ‖ Comparison of the solubilities of $LiNO_3, NaNO_3$ and KNO_3; ∘, $LiNO_3$; ⋆, $NaNO_3$; △, KNO_3; dashed lines represents the respective description of the solubilities with equation 4.10

exist (e.g. diagonal relationship with magnesium, high solubility in polar organic solvents (46)). Due to the small ionic radius, the lithium cation has a high charge density what results in a stronger attraction of the electrons of the corresponding anion. Therefore, considering the proposed association and precipitation mechanism (cf. Eq. 4.2), the formed associated LiCl complex is likely to have a more covalent bonding structure than the NaCl and KCl complex. This results in a more difficult hydration and a lower solubility for LiCl since partial charges of the molecules are not as pronounced as for NaCl and KCl. Nevertheless, this does not explain the higher solubilities of LiCl in comparison to NaCl and KCl at lower densities. To investigate the actual hydration structure of LiCl and compare it to NaCl and KCl, molecular modeling and spectrographic measurements (Infrared, Raman) (47) are considered as possible tools. The application of these tools could give a verification of the assumptions made above or offer a different explanation for this phenomenon.

Relation of model parameters and salt properties

Due to the results presented above, a possible relation between the radius of the salt molecule and the model parameters of Eq. 4.10 is investigated. To extend the available

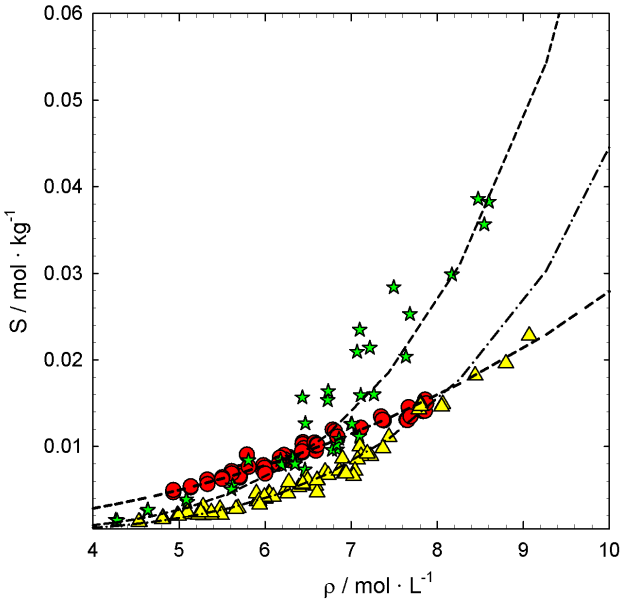

Figure 4.11 ‖ Comparison of the solubilities of $\mathrm{LiCl}, \mathrm{NaCl}$ and KCl; ∘, LiCl; ⋆, NaCl; △, KCl; dashed lines represent the respective description of the solubilities with Eq. 4.10

Table 4.5 ‖ Model parameters of the salts CuO, PbO, and KOH for Eq. 4.10 (37; 48; 49)

Salt	A / $J \cdot mol^{-1}$	B / $J \cdot mol^{-1} \cdot K^{-1}$	n / -
CuO	23749	-103.68	1.339
PbO	27901	-57.97	1.971
KOH	13369	-81.10	3.244

data and to have a greater significance, parameters of three additional monovalent salts ($\mathrm{CuO}, \mathrm{PbO}, \mathrm{KOH}$) are added to the parameters presented in the section before. These parameters were obtained from solubility data available in literature (37; 48; 49) and can be found in Table 4.5. The experimental data of *Hearn et al.* for CuO has to be treated carefully since large scattering occurs throughout the data set (48).

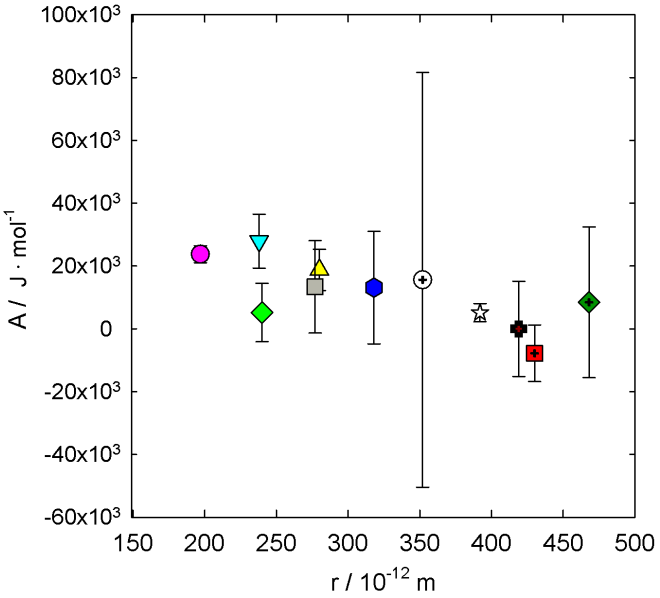

Figure 4.12 ‖ Parameter A (cf. Eq. 4.10) as a function of the molecule radius; ∘, CuO; ▽, PbO; ⋄, LiCl; □, KOH; △, NaCl; ⬡, KCl; ⊕, $\mathrm{LiNO_3}$; ⋆, $\mathrm{NaNO_3}$; ⊞, $\mathrm{KNO_3}$; the vertical bars represent the numerical uncertainty of the parameter resulting from the fitting procedure

In Figure 4.12, 4.13 and 4.14 the model parameters are presented as a function of the molecule radius including the standard deviations (cf. Tbl. 4.2 and 4.4). The radii were obtained from the corresponding crystal radii (40). For parameter A, which is a direct

function of the temperature, and parameter B, which is correlated to the parameter ΔH due to the chosen mathematical approach (cf. Eq. 4.10), the magnitude of the standard deviations are primarily resulting from the temperature range that is covered in the experimental data. This is most prominent for $LiNO_3$ where only a range from 663 to 679 K was investigated. Therefore, additional experiments for $LiNO_3$ are advisable to correct these deviations.

For parameters A and B, a linear correlation between the radius and the parameter can be found. Both parameters increase with decreasing radius.

For the parameter *n*, two groups can be distinguished (Group I: $NaCl$, KCl, $LiNO_3$, $NaNO_3$, KNO_3; group II: CuO, PbO, $LiCl$, KOH). Group I shows a linear correlation with an increasing coordination number for a smaller molecule radius. This behavior has been discussed above for the nitrate salts in regard of the overall solubility, where the coordination number was taken as an indicator for the solubility. As can be seen in Fig. 4.14, this behavior can also be found for KCl and $NaCl$.

Group II shows a different tendency. Their coordination number show an increasing trend with an increasing radius. CuO, PbO, KOH and $LiCl$ (as discussed above) have a more covalent binding character in comparison to the more ionic compounds in group

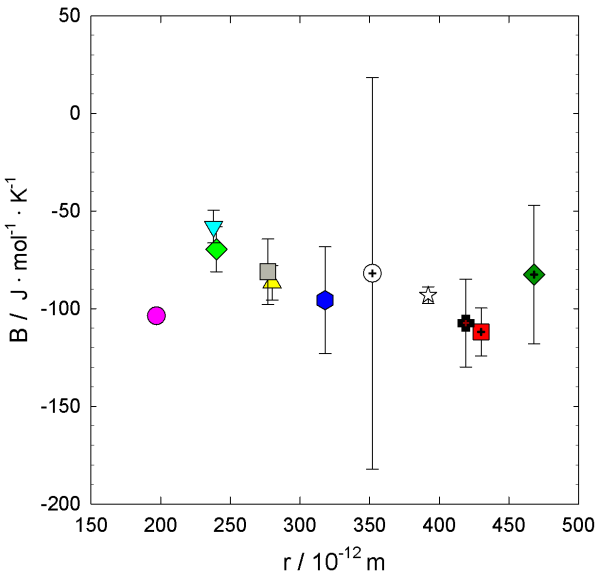

Figure 4.13 ‖ Parameter B (cf. Eq. 4.10) as a function of the molecule radius; ○, CuO; ▽, PbO; ◇, $LiCl$; □, KOH; △, $NaCl$; ⬡, KCl; ⊕, $LiNO_3$; ⋆, $NaNO_3$; ⊞, KNO_3; the vertical bars represent the numerical uncertainty of the parameter resulting from the fitting procedure

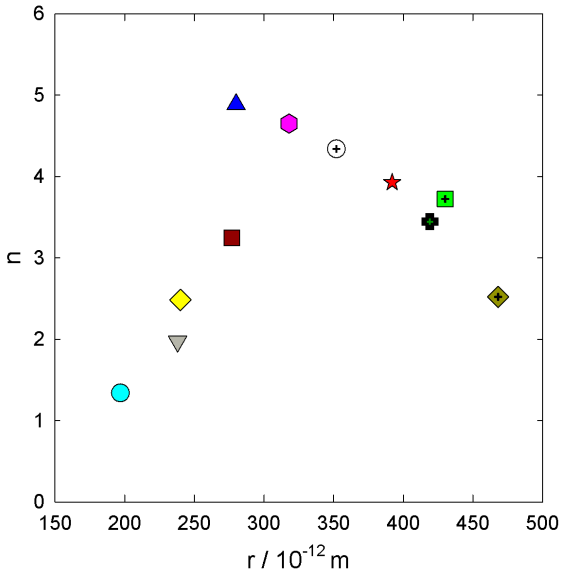

Figure 4.14 ‖ Parameter n (cf. Eq. 4.10) as a function of the molecule radius; ∘, CuO; ▽, PbO; ⋄, LiCl; □, KOH; △, NaCl; ⬡, KCl; ⊕, $\mathrm{LiNO_3}$; ⋆, $\mathrm{NaNO_3}$; ⊞, $\mathrm{KNO_3}$; the vertical bars represent the numerical uncertainty of the parameter resulting from the fitting procedure

I. Therefore, the difference in electronegativity between the salt components can be taken as an indicator for ionic / covalent character (e.g. difference in electronegativity of NaCl: 3.16 (Cl) ; 0.93 (Na); difference in electronegativity of CuO: 3.44 (O) ; 1.90 (Cu)). The more covalent character results in less pronounced local charges which makes it more difficult to establish hydrogen bonds between the salt molecule and the surrounding water. Therefore, less water molecules are bound to the salt molecule resulting in a lower coordination number. It can be concluded from this behavior that the coordination number is not only depending on the molecule radius, but also on the binding character of the compound.

In Figure 4.15, the solubility of the salts mentioned above at 673 K and 25 MPa are presented as a function of the coordination number. As can be seen, increasing solubility correlates in an exponential manner with an increasing coordination number (with exception of CuO). Therefore, these relations between the radius, the binding character and the parameters of the model can be used to predict to a certain degree the solubilities of salts and the parameters of the model where no or little property data is available in open literature.

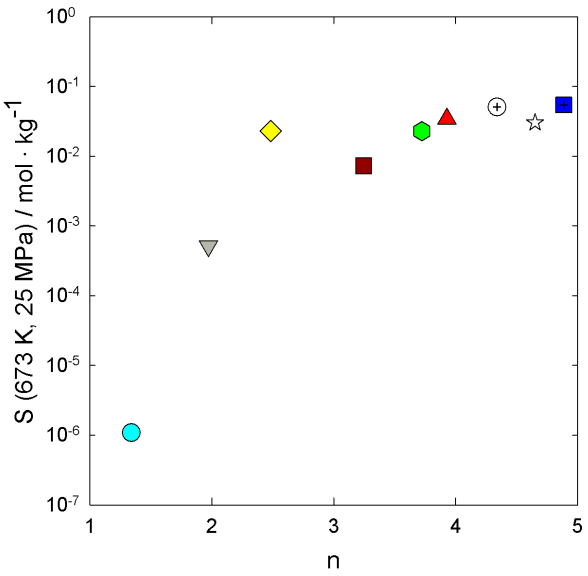

Figure 4.15 ‖ Solubility at 673 K and 25 MPa as a function of the coordination number; ∘, CuO; ▽, PbO; ⋄, $LiCl$; □, KOH; ⬡, $NaNO_3$; △, KNO_3; ⊕, $LiNO_3$; ⋆, KCl; ⊞, $NaCl$

4.5 Conclusions

In the course of this work, a systematical study of the solubilities of three alkali chloride salts ($LiCl$, $NaCl$, KCl) and three alkali nitrate salts ($LiNO_3$, $NaNO_3$, KNO_3) was performed. The study was performed in one setup using one method. The investigated range was from 653 to 693 K and from 18 to 23.5 MPa.

The solubilities of each group were compared with each other. For alkali nitrates, a clear tendency in the solubility in correspondence with the molecule radius could be determined ($LiNO_3 > NaNO_3 > KNO_3$). For alkali chlorides, a similar tendency could not be determined due to the anomalous behavior of $LiCl$. Considering the parameters obtained from the model, it can be concluded that a high solubility in supercritical water correlates with the ability of the molecule to establish as many hydrogen bonds with the surrounding water and to maintain a hydration sphere. This results in a higher coordination number.

A comparison of the radii of the inorganic compounds with the parameters obtained by Eq. 4.10 showed that a linear relation exist between the enthalpy and entropy parameter and the radius. The coordination number was found to be additionally depending on the binding character of the molecule.

The experiments revealed that next to the precipitation of alkali chlorides and nitrates several side reactions take place. During all experiments a drop in pH from 4 to 6 was found resulting from a hydrolysis reaction. During the experiments with alkali nitrates, small concentrations of nitrite were found resulting from the decomposition of the nitrate.

4.6 Acknowledgements

The authors thank Sonia Touzot for her contribution to the experimental part of this work. Additionally the authors thank Janneke Tempel and Jelmer Dijkstra for their contribution in the analysis of the samples.

This work was performed in the TTIW-cooperation framework of Wetsus, centre of excellence for sustainable water technology (www.wetsus.nl). Wetsus is funded by the Dutch Ministry of Economic Affairs, the European Union Regional Development Fund, the Province of Fryslân, the City of Leeuwarden, and the EZ/Kompas program of the 'Samenwerkingsverband Noord-Nederland'. The authors like to thank the participants of the research theme *Salt* for their financial support.

4.7 References

[1] T. Clifford, Fundamentals of Supercritical Fluids, Oxford University Press, 1999.

[2] C. Aymonier, A. Loppinet-Serani, H. Reveron, Y. Garrabos, F. Cansell, Review of supercritical fluids in inorganic materials science, The Journal of Supercritical Fluids 38 (2) (2006) 242.

[3] F. Cansell, S. Rey, P. Beslin, Continous catalytic reactions in supercritical fluids processing: Applications to polymers and waste treatment, Revue de l'institut francais du petrole 1 (1998) 71 – 98.

[4] C. Erkey, Supercritical carbon dioxide extraction of metals from aqueous solutions: A review, The Journal of Supercritical Fluids 17 (3) (2000) 259.

[5] J. Fages, H. Lochard, J.-J. Letourneau, M. Sauceau, E. Rodier, Particle generation for pharmaceutical applications using supercritical fluid technology, Powder Technology 141 (3) (2004) 219.

[6] J. R. Hyde, P. Licence, D. Carter, M. Poliakoff, Continuous catalytic reactions in supercritical fluids, Applied Catalysis A: General 222 (1-2) (2001) 119.

[7] A. B. Jarzebski, J. J. Malinowski, Potentials and prospects for application of supercritical fluid technology in bioprocessing, Process Biochemistry 30 (4) (1995) 343.

[8] J. Jung, M. Perrut, Particle design using supercritical fluids: Literature and patent survey, The Journal of Supercritical Fluids 20 (3) (2001) 179.

[9] M. van der Kraan, M. V. Fernandez Cid, G. F. Woerlee, W. J. T. Veugelers, G. J. Witkamp, Dyeing of natural and synthetic textiles in supercritical carbon dioxide with disperse reactive dyes, The Journal of Supercritical Fluids 40 (3) (2007) 470–476.

[10] M. J. E. van Roosmalen, M. van Diggelen, G. F. Woerlee, G. J. Witkamp, Dry-cleaning with high-pressure carbon dioxide–the influence of mechanical action on washing-results, The Journal of Supercritical Fluids 27 (1) (2003) 97–108.

[11] A. Kruse, E. Dinjus, Hot compressed water as reaction medium and reactant: Properties and synthesis reactions, The Journal of Supercritical Fluids 39 (3) (2007) 362.
[12] E. Lester, P. Blood, J. Denyer, D. Giddings, B. Azzopardi, M. Poliakoff, Reaction engineering: The supercritical water hydrothermal synthesis of nano-particles, The Journal of Supercritical Fluids 37 (2) (2006) 209.
[13] P. E. Savage, Heterogeneous catalysis in supercritical water, Catalysis Today 62 (2-3) (2000) 167.
[14] G. J. DiLeo, P. E. Savage, Catalysis during methanol gasification in supercritical water, The Journal of Supercritical Fluids 39 (2) (2006) 228.
[15] M. J. Antal, S. G. Allen, D. Schulman, X. Xu, R. J. Divilio, Biomass gasification in supercritical water, Ind. Eng. Chem. Res. 39 (11) (2000) 4040–4053.
[16] W. Feng, H. J. van der Kooi, J. de Swaan Arons, Biomass conversions in subcritical and supercritical water: Driving force, phase equilibria, and thermodynamic analysis, Chemical Engineering and Processing 43 (12) (2004) 1459.
[17] Y. Matsumura, T. Minowa, B. Potic, S. R. A. Kersten, W. Prins, W. P. M. van Swaaij, B. van de Beld, D. C. Elliott, G. G. Neuenschwander, A. Kruse, M. J. Antal, Biomass gasification in near- and super-critical water: Status and prospects, Biomass & Bioenergy 29 (4) (2005) 269–292, 0961-9534.
[18] E. F. Gloyna, L. Li, Supercritical water oxidation: An engineering update, Waste Management 13 (5-7) (1993) 379.
[19] H. Schmieder, J. Abeln, Supercritical water oxidation: State of the art, Chemical Engineering & Technology 22 (1999) 903 – 908.
[20] B. Veriansyah, T.-J. Park, J.-S. Lim, Y.-W. Lee, Supercritical water oxidation of wastewater from LCD manufacturing process: Kinetic and formation of chromium oxide nanoparticles, The Journal of Supercritical Fluids 34 (1) (2005) 51.
[21] K. Prikopsky, B. Wellig, P. R. von Rohr, SCWO of salt containing artificial wastewater using a transpiring-wall reactor: Experimental results, The Journal of Supercritical Fluids 40 (2) (2007) 246.
[22] N. Lummen, B. Kvamme, Kinetics of NaCl nucleation in supercritical water investigated by molecular dynamics simulations, Physical Chemistry Chemical Physics 9 (25) (2007) 3251–3260.
[23] D. E. Knox, Solubilities in supercritical fluids, Pure Applied Chemistry 77 (2005) 513 – 530.
[24] F. J. Armellini, J. W. Tester, Solubility of sodium chloride and sulfate in sub- and supercritical water vapor from 450-550 °C and 100-250 bar, Fluid Phase Equilibria 84 (1993) 123.
[25] T. Yamaguchi, M. Yamagami, H. Ohzono, H. Wakita, K. Yamanaka, Chloride-ion hydration in supercritical water by neutron diffraction, Chemical Physics Letters 252 (5-6) (1996) 317–321.
[26] T. Yamaguchi, Structure of subcritical and supercritical hydrogen-bonded liquids and solutions, Journal of Molecular Liquids 78 (1-2) (1998) 43–50.
[27] P. A. Marrone, M. Hodes, K. A. Smith, J. W. Tester, Salt precipitation and scale control in supercritical water oxidation–part B: Commercial/full-scale applications, The Journal of Supercritical Fluids 29 (3) (2004) 289.
[28] M. Hodes, P. A. Marrone, G. T. Hong, K. A. Smith, J. W. Tester, Salt precipitation and scale control in supercritical water oxidation – part A: Fundamentals and research, The Journal of Supercritical Fluids 29 (3) (2004) 265.
[29] A. A. Peterson, P. Vontobel, F. Vogel, J. W. Tester, In situ visualization of the performance of a supercritical-water salt separator using neutron radiography, Journal of Supercritical Fluids 43 (3) (2008) 490–499.
[30] P. Kritzer, N. Boukis, E. Dinjus, Factors controlling corrosion in high-temperature aqueous solutions: a contribution to the dissociation and solubility data influencing corrosion processes, The Journal of Supercritical Fluids 15 (3) (1999) 205.
[31] P. J. Crooker, K. S. Ahluwalia, Z. Fan, J. Prince, Operating results from supercritical water oxidation plants, Industrial & Engineering Chemistry Research 39 (12) (2000) 4865–4870.
[32] P. Kritzer, Corrosion in high-temperature and supercritical water and aqueous solutions: A review,

The Journal of Supercritical Fluids 29 (1-2) (2004) 1.
[33] T. M. Hayward, I. M. Svishchev, R. C. Makhija, Stainless steel flow reactor for supercritical water oxidation: Corrosion tests, The Journal of Supercritical Fluids 27 (3) (2003) 275.
[34] I. Leusbrock, S. Metz, G. Rexwinkel, G. F. Versteeg, Quantitative approaches for the description of solubilities of inorganic compounds in near-critical and supercritical water, The Journal of Supercritical Fluids 47 (2) (2008) 117–127.
[35] J. Chrastil, Solubility of solids and liquids in supercritical gases, Journal Of Physical Chemistry 86 (15) (1982) 3016–3021.
[36] C. Yokoyama, A. Iwabuchi, S. Takahashi, K. Takeuchi, Solubility of PbO in supercritical water, Fluid Phase Equilibria 82 (1993) 311.
[37] K. Sue, Y. Hakuta, R. L. Smith, T. Adschiri, K. Arai, Solubility of Lead(II) Oxide and Copper(II) Oxide in Subcritical and Supercritical water, J. Chem. Eng. Data 44 (6) (1999) 1422–1426.
[38] W. Wagner, The IAPWS formulation 1995 for the thermodynamic properties of ordinary water substance for general and scientific use, Journal of Physical and Chemical Reference Data 31 (2) (1999) 387.
[39] D. R. Ride, CRC Handbook of Chemistry and Physics, CRC Press, 2004.
[40] R. D. Shannon, Revised effective ionic-radii and systematic studies of interatomic distances in halides and chalcogenides, Acta Crystallographica Section A 32 (SEP1) (1976) 751–767.
[41] P. Dell'Orco, H. Eaton, T. Reynolds, S. Buelow, The solubility of 1:1 nitrate electrolytes in supercritical water, The Journal of Supercritical Fluids 8 (3) (1995) 217.
[42] H. Higashi, Y. Iwai, K. Matsumoto, Y. Kitani, F. Okazaki, Y. Shimoyama, Y. Arai, Measurement and correlation for solubilities of alkali metal chlorides in water vapor at high temperature and pressure, Fluid Phase Equilibria 228-229 (2005) 547.
[43] J. F. Galobardes, D. R. Vanhare, L. B. Rogers, Solubility of sodium-chloride in dry steam, Journal of Chemical and Engineering Data 26 (4) (1981) 363–366.
[44] A. A. Chialvo, P. T. Cummings, H. D. Cochran, J. M. Simonson, R. E. Mesmer, $Na^+ - Cl^-$ ion-pair association in supercritical water, Journal of Chemical Physics 103 (21) (1995) 9379–9387.
[45] G. Sciáini, E. Marceca, R. Fernández-Prini, Is ammonia a better solvent than water for contact ion pairs?, J.Phys.Chem. B 112 (38) (2008) 11990–11995.
[46] A. M. Sapse, P. R. Schleyer, Lithium Chemistry: A Theoretical and Experimental Overview, Wiley-Interscience, 1995.
[47] T. Tassaing, P. Garrain, D. Bégué, I. Baraille, On the cluster composition of supercritical water combining molecular modeling and vibrational spectroscopic data, Proceedings of the 9th International Symposium on Supercritical Fluids.
[48] B. Hearn, M. R. Hunt, A. Hayward, Solubility of cupric oxide in pure subcritical and supercritical water, J. Chem. Eng. Data 14 (4) (1969) 442–447.
[49] W. T. Wofford, P. C. Dellorco, E. F. Gloyna, Solubility of potassium hydroxide and potassium phosphate in supercritical water, Journal of Chemical and Engineering Data 40 (4) (1995) 968–973.